International Journal of Modern Manufacturing Technologies
ISSN 2067–3604, Vol. XIV, No. 3 / 2022
https://doi.org/ 10.54684/ijmmt.2022.14.3.181

NUMERICAL SIMULATION FOR THE MOTION RESPONSE OF AN OFFSHORE AHTS SHIP IN REGULAR AND IRREGULAR WAVES

Sandita Pacuraru, Leonard Domnisoru, Adham Bekhit

"Dunarea de Jos" University of Galati, Faculty of Naval Architecture
47 Domneasca Street, 800008, Galati, Romania

Corresponding author: Adham Bekhit, adham.bekhit@ugal.ro

Abstract: This study aims at predicting the hydrodynamic response of an offshore AHTS vessel in regular and irregular waves. The study focuses on predicting the six degrees of freedom responses for ship in the operation condition when ship speed is equal to zero, at various heading angles (0, 45, 90, 135, 180, 225, 270, and 315˚) and for several wave frequencies (0.02~2.0 rad/s). The numerical simulation is carried out using the 3D diffraction/radiation Hydrostar software that is based on potential theory to predict the wave-body interactions. All the hydrostatics, loading and sailing aspects are initially estimated, and then introduced as an input in the simulation process corresponding to the ship speed and heading directions. For the irregular sea simulations, the ITTC spectrum is used to describe the wave for a generic case study in the Black Sea in order to make the study feasible for offshore applications in operational conditions. Further investigations are made using the ISIS_CFD viscous flow solver of the FINETM/Marine software (only for regular waves) to compare the obtained results. The results are presented for the ship response with a considered accuracy based on the previous validations performed by the authors for similar ships.
Key words: AHTS, 3D potential theory, regular waves, irregular waves, seakeeping.

1. INTRODUCTION

Hydrodynamic performance of ships in waves has a significant importance due to its possible impact on ship stability, operability, and at a certain stage, safety and survivability. It is crucial to take into considerations the ship responses in wave in order to insure safe operations and optimum performance by means of design and operational considerations. Numerical simulation plays a significant role in this scope to predict the ship seakeeping performance in regular and irregular waves with a satisfying level of accuracy. Potential flow-based methods can be considered as the work horse of seakeeping simulations for the past five decades. This is related to its simplicity, and efficiency in terms of the CPU time needed to obtain the solution with a satisfactory level of accuracy. The linear potential flow seakeeping solvers based on the strip theory, source distribution method, panel method and more recently enhanced unified theory, were widely used by ship researchers [1]; Nevertheless, due to limitations of the physical modelling principles, the solutions had some drawbacks determined mainly by the neglected viscous effect [2]. Most recently, the viscous flow solvers based on Unsteady Reynolds-Averaged Navier-Stokes Equations (URANSE) and seldom based on Large Eddy Simulations (LES) or Detached Eddy Simulations (DES) approaches took place in the seakeeping performance prediction domain. They obviously have an advantage over the BEM methods when talking about large amplitude motions, capsizing, breaking waves and green water, etc. Unfortunately, the associated cost and computational time is very significant. This study is an attempt by the authors to investigate the seakeeping behaviour of an offshore Anchor Handling Tug Supply (AHTS) vessel during the operation conditions, where the ship speed is equal to zero and at multiple heading angles. Similar attempts by the author based on the BEM method was presented in [3], while a similar comparison between BEM and URANSE for the seakeeping performance of a tanker was reported in [4]. URANSE-based approach was conducted for the model scale ships of a tanker, and a surface combatant can be found in [5, 6].

The analysis conditions in this study can be categorized based on two approaches; the first is a 3D diffraction/radiation potential theory using the Hydrostar software developed and provided by Bureau Veritas [7] while the second approach is based on URANSE using the viscous flow solver ISIS-CFD of the FINE™/Marine software provided under the Cadence suit (formerly, NUMECA). The first approach is concerned with predicting the response of the ship in both regular and irregular waves at various operation conditions including different heading angles. Nonetheless, the second approach is concerned with only one case study aimed at comparing the obtained results from the

potential theory with those from the viscous flow concept, paying a closer attention to the oscillatory (heave, pitch and especially roll) motions. This study stands as an initial step for further investigations that will be conducted in the near future.

2. GEOMETRY AND ANALYSIS CONDITIONS

The current study is applied on a full scale AHTS ship whose length is LPP=60 m and draft is T=4.35 m, the full characteristics of the ship are summarized in Table 1. The geometry of the ship is appended with a central skeg as depicted in Figure 1. The ship has two speeds V=0 and 12.5 Knots, the first is for operational tasks nearby the offshore platforms and the last is for free sailing condition. Only the operational condition zero speed is taken into consideration during the numerical simulation process in regular and irregular waves.

Table 1. Principal particulars for the AHTS

Parameter	Unit	Value
Length (overall), L_{OA}	[m]	71.0
Length (waterline), L_{WL}	[m]	66.0
Length, L_{PP}	[m]	60.0
Beam, B	[m]	13.6
Draft, T	[m]	4.35
Depth (molded), D_m	[m]	7.96
Depth (maximum), D_{max}	[m]	16.4
Displacement, Δ	[t]	2277
Block coefficient, C_B	-	0.626

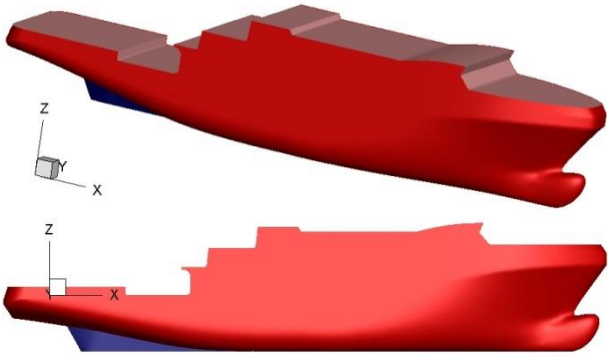

Fig. 1. AHTS ship model geometry

The analysis conditions including the ship speed, wave frequency and heading angles are tabulated in Table 2, while the heading notations are schematically represented in Figure 2.

Table 2. Simulation cases summary

Ship Velocity	Potential Flow Simulation						Viscous Flow Simulation		
V [knots]	C1 (regular waves)			C2 (irregular waves)			C3 (regular waves)		
	ω [rad/s]	ζ [m]	μ [°]	ω [rad/s]	ζ [m]	μ [°]	ω [rad/s]	ζ [m]	μ [°]
0	0.02~2	1	0~315	0.02~2	1	0~315	0.8	1	180

where ω represents the wave frequency, ζ wave amplitude and μ stands for the ship's heading angle. It is worth mentioning that the step chosen for frequency $\Delta\omega$=0.02 rad/s, while the step chosen for the ship's heading angle $\Delta\mu$=15°.

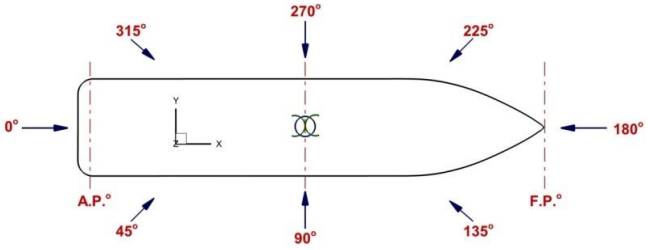

Fig. 2. Schematic representation for ship's heading angle μ [7]

3. NUMERICAL FRAMEWORK

3.1 BEM Boundary Element Method simulation

3.1.1. Numerical solver

The potential flow simulation is carried out using the Hydrostar software developed by Bureau Veritas. The software provides a complete solution of first order problem of wave diffraction and radiation and also the Quadratic Transfer Function (QTF) of second order low-frequency wave loads for floating body with or without forward speed in deep water and in finite water depth [7]. The Green theorem is used to derive the integral equation of the first-order boundary value problem.

3.1.2. Governing equations

Under the potential flow assumption, the flow is incompressible, inviscid and irrotational. The velocity can be obtained from the velocity potential function Φ as:

$$V = \nabla\phi \qquad (1)$$

Hence, the potential function satisfies the Laplace condition, hence the conservation of mass equation can be written as:

$$V^2\phi = 0 \qquad (2)$$

The flow is assumed to be (fairly perfect fluid) as described by Guevel (1982) [8]; now, the momentum equation is written as:

$$(\partial/\partial t + V\nabla)V = -\nabla(P_r/\rho + gz) - \mu V \qquad (3)$$

where P_r is the pressure and g is the gravitational acceleration. Based on equation (1), the Bernoulli equation is written as follows:

$$P_r/\rho + gz + \phi_t + \nabla\phi\nabla\phi/2 + \mu\phi = C(t) \qquad (4)$$

$C(t)$ is an arbitrary function and usually omitted.

At the free surface, the dynamic condition requires that the pressure given by Bernoulli equation (4) should be equal to the atmospheric pressure. The kinematic condition refers to the fact that a particle in motion at the free surface stays always on the same surface. Considering the dynamic and kinematic conditions, the relation given below is obtained:

$$g\phi_z + \phi_{tt} + \mu\phi_t + 2\nabla\phi\nabla\phi_t + \nabla\phi\cdot\nabla(\nabla\phi\nabla\phi)/2 = 0 \quad (5)$$

and the free surface can be written:

$$\varepsilon(p,t)g = -\phi_t - \nabla\phi\nabla\phi/2 - \mu\phi \quad (6)$$

Since the ship is sailing in waves, the regular wave has the following expression:

$$\zeta(X,Y,t) = a\cos\left\{\omega t - k\begin{bmatrix}(X - X_{cal})\cos\beta + \\ (Y - Y_{cal})\sin\beta\end{bmatrix}\right\} \quad (7)$$

where ζ is the wave elevation, a is the wave amplitude, ω is wave frequency, t stands for the time, β is the wave heading angle and k is the wave number. The ship motion will have the expression:

$$U(t) = u\cos(\omega t + \phi) \quad (8)$$

where u is the amplitude of the motion and ϕ is the phase.

For irregular waves, the ITTC wave spectrum is chosen for a maximum operational condition at Beaufort scale 6, where the significant wave height $H_S = 4m$. The wave spectrum $S_\zeta(\omega)$ and the encounter spectrum $S_R(\omega_e)$ equations are described as:

$$S_\zeta(\omega) = \frac{A}{\omega^5}e^{\frac{B}{\omega^4}} \quad (9)$$

where $A = 0.0081g^2$ & $B = \frac{3.11}{H_S^2}$.

$$S_R(\omega_e) = RAO^2 S_\zeta(\omega) \quad (10)$$

where the suffix R refers to the response, while $\omega_e = \omega\left[1 = \frac{\omega V}{g}\cos\mu\right]$; and consequently, $\omega_e = \omega$ when $V = 0$.

3.1.3. Simulation Grid

The ship geometry is checked for any possible geometrical issues (such as discontinuity, surface deformations, twisting, etc.) that may affect the simulation quality; afterwards the ship is cut at the free-surface level. The geometry is then introduced into a mesh generator to create the simulation panels. The generated panels geometry is depicted in Figure 3, while the number of nodes for both simulation cases are tabulated in Table 3.

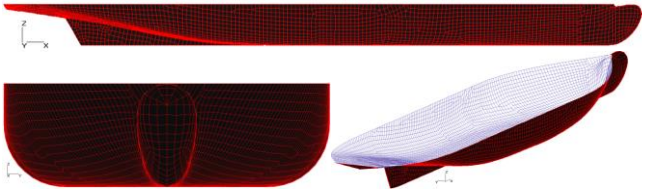

Fig 3. Panels configuration for ships' profile, front and 3D views, respectively

Table 3. Number of panels and nodes for simulation cases

Simulation Cases	Number of Nodes	Number of Panels
C1 & C2	3449	3207

3.1.4. Solution strategy and available resources

The ship is considered at the full loading case in the operation condition (i.e. zero-speed), and the heading angles between 0˚ and 315˚ with a step of 15˚ degrees and the wave frequency ranging from 0.02 to 2 rad/s with a step 0.02. The linear viscous damping is set at 8%. The ship is investigated in the regular wave condition and then the RAO response data are used to generate the ship response in irregular waves according to equations (9 & 10). The simulation is performed on a 16 cores PC with 3.0G Hz I7 processor and 32 GB RAM. The total physical time for the simulation is about 4 hours.

3.2 URANSE Simulation

3.2.1. Numerical solver

The viscous flow simulation is carried out using the ISIS-CFD solver of the FINETM/Marine software. The solver is based on the finite volume method to build the spatial discretization of the transport equation to solve the unsteady Reynolds-Averaged Navier-Stokes Equations (URANSE) [9]. The spatial discretization is face-based, which makes the solver suitable for using unstructured grids to provide flexibility for complex ship geometries and appendages. The temporal discretization is cell-centred based on a second order three-level scheme. The velocity field is obtained from the momentum equation; while the pressure is extracted from the mass constraint or continuity equation transformed into a pressure equation. The velocity and pressure coupling is carried out using a Rhie and Chaw SIMPLE type algorithm [10]. Closure to turbulence is achieved through the blended Menter's Shear Stress Transport K-ω SST turbulence model. The free-surface is captured through a multi-phase (air-water)

interface using the Volume of Fluid (VOF) method. Convection and diffusion terms in the governing equations are discretized using second-order upwind and central differencing scheme, respectively.

3.2.2. Governing equations

The time averaged continuity and momentum equations for the incompressible flow with external forces, can be written in tensor form, in the Cartesian coordinate system as:

$$\frac{\partial\left(\rho\overline{u_i}\right)}{\partial x_i} = 0 \qquad (11)$$

$$\frac{\partial\left(\rho\overline{u_i}\right)}{\partial t} + \frac{\partial}{\partial x_j}\left(\rho\overline{u_i}\,\overline{u_j} + \rho\overline{u_i}'\overline{u_j}'\right) = \frac{\partial\overline{p}}{\partial x_i} + \frac{\partial\overline{\tau}_{ij}}{\partial x_j} \qquad (12)$$

where $\bar{u}_i$ is the relative averaged velocity vector of flow between the fluid and the control volume, $\overline{u_i'u_j'}$ is the Reynolds stresses, $\bar{p}$ is the mean pressure and $\bar{\tau}_{ij}$ is the mean viscous stress tensor components for Newtonian fluid under the incompressible flow assumption, and it can be expressed as:

$$\bar{\tau}_{ij} = \mu\left(\frac{\rho\overline{u_i}}{\partial x_j} + \frac{\rho\overline{u_j}}{\partial x_i}\right) \qquad (13)$$

3.2.3. Computational domain and boundary conditions

The computational domain is having a rectangular prism configuration as depicted in Figure 2. The main dimensions of the computational domain in (x–y–z) direction are ($9.0L_{PP}$–$4.0L_{PP}$–$6.0L_{PP}$), where, as illustrated in Figure 4. The inflow boundary is located at 2.75 L_{pp} upstream, the exit boundary is located at 5.25 L_{pp} downstream, $2.0L_{pp}$ laterally on both sides, the top boundary is located at $2.0L_{pp}$ above the non-disturbed free-surface level, which is located at z=5.1m from the baseline of the ship, as it is highlighted in blue in Figure 4. Unlike the common analysis where the flow starts at the inflow boundary, a new option is added for ship simulation at speed V=0 m/s to start the wave propagation at a distance from the inflow boundary (here the distance is at 0.75 L_{pp}, which is quoted in Figure 4 as the internal wave generator. It is also recommended to have a sufficient wave propagation zone before encountering the ship at the forward perpendicular with at least two times the wave length. In order to limit the number of grid cells, and especially where the ship is sailing at zero speed, the free-surface refinement zone dedicated for capturing the wave after the ship is only 1.0 L_{pp}. Afterwards the zone on the free-surface is gradually coarsened to provide a sufficient wave damping to avoid reflections from the exit boundary. For a similar reason (i.e. to avoid reflections on the side boundaries) a symmetry condition is posed on both domain sides.

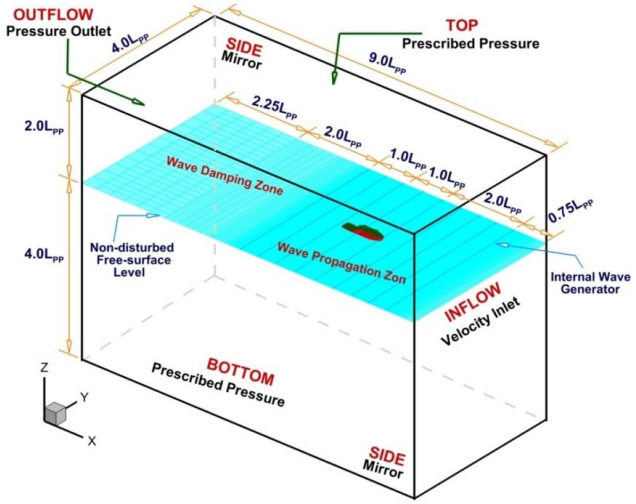

Fig. 4. Computational domain, dimensions and boundary conditions

The boundary conditions are imposed either Dirichlet or Neumann boundary condition as shown in Figure 4. All the principal dimensions and coordinates are introduced with respect to Cartesian coordinate system with an earth fixed reference frame situated at the point (0, 0, and 0) located at the intersection between the ship Aft Perpendicular A.P. and base line, while ship response is measured by tracing the C.O.G. The reference ship-wave encounter line is located at the Forward Perpendicular F.P. which will be used to define the position of the wave with respect to the ship.

3.2.4. Discretization Grid

The computational grids are generated using the automatic unstructured hexahedral grid generator HEXPRESS™ provided in the Fine™/MARINE package. The detailed number of grid cells for every simulation case is tabulated in Table 4, while Figure 5 shows the computational grid for the case number C3, as it was previously described in Table 2. The free-surface refinement consists of two refinement levels; the first imposes a global surface refinement at the undisturbed water level for the entire domain with relatively coarser grid, while the second imposes a finer grid in the wave propagation zone in order to capture more details and avoid any possible numerical damping. The refinement in the wave propagation zone is made such that the cell size provides 60 grid cells per wave length in x- and y-directions ($\Delta x=\Delta y=2\pi Fr^2L_{WL}/60$), where Froude number in this case is computed based on the wave celerity because the ship speed is zero. On the other hand, in z-direction, the thickness of the refinement zone is chosen as three times the wave height, divided in two equal segments above and

beneath the undisturbed free-surface level. The cell size in *z*-direction for the free-surface refinement sector is chosen as $\Delta z=H/20$, where H refers to the wave height.

Table 4. Number of grid cells for simulation cases

	C3
Number of grid cells (M)	9.362

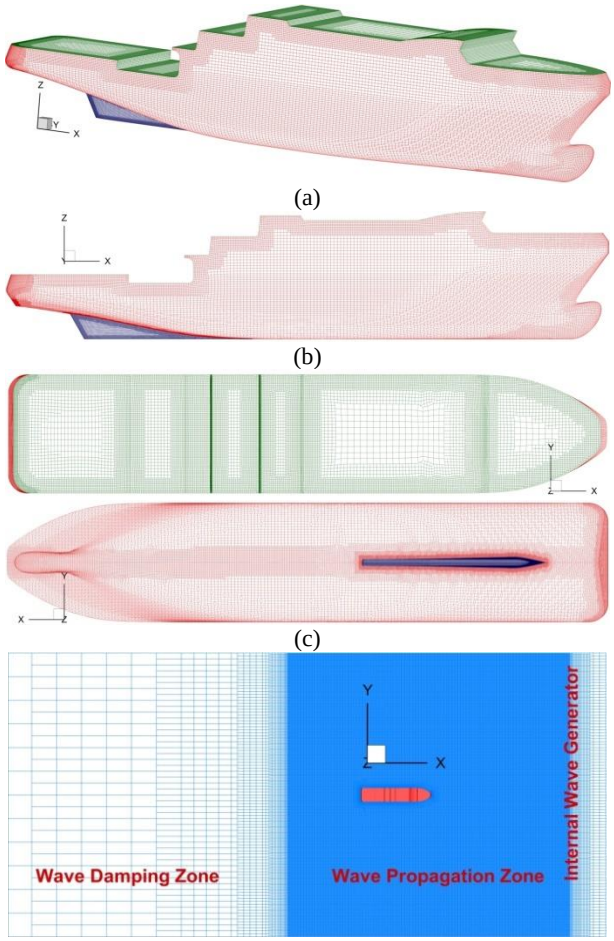

(a) (b) (c) (d)

Fig. 5. Discretization grids showing: (a) 3D view, (b) side view, (c) top and bottom view and (d) free-surface refinement

3.2.5. Solution strategy and available resources

The CFD simulations are performed on a High Performance Computing (HPC) system with available 120 cores at 2.5 up to 3.3 GHz. The simulation is performed for a sufficient duration to encounter 15 waves. The wave is generated using an internal wave generator locates at a distance 0.75 L_{pp} and 2.0 L_{pp} from the ship forward perpendicular, in order to provide sufficient time in the beginning of the simulation for the ship before encountering the wave to avoid overshoots and numerical instabilities in the beginning of the simulation. The ship speed is set to zero, while the flow speed corresponds to the wave celerity estimated by the equation $C_w = \sqrt{g\lambda/2\pi}$ where g represents the gravity acceleration and λ represents the wave length. 12 non-linear iterations are used with a fourth order convergence criteria and a time step Δt chosen based on the ITTC recommended procedures for seakeeping CFD simulations to provide 200 iterations per wave period [11]. Similar values were used in [5, 6] and showed sufficient accuracy. The physical simulation time is recorded for both simulations between 153 and 218 hours for head and oblique waves, respectively. This may conclude that this simulation is very expensive and time consuming; yet, the viscous flow provides more details that are difficult to be captured with other methods. This is why only two cases were performed for this simulation for comparison purposes, since the method is still not feasible for multiple cases, frequencies and encounter angles.

4. RESULTS AND DISCUSSIONS

4.1 BEM results

The simulation is performed for the ship at zero speed stetting the heading angle μ=0˚ to 315˚ with a step of 15˚, while the circular wave frequency ω is varied in range of 0.02 to 2 rad/s. The regular wave has an amplitude of a_w=1m and the wave height H=2m. The Response Amplitude Operators (RAO) measure units are m/m for the translation degrees and degrees/m for the rotational motion. The three translation degrees are surge, sway and surge motion, along X, Y and Z axis respectively. Similarly, the rotation around X, Y and Z axis are roll, pitch and yaw motions respectively. The results are presented in the following subsection for ship in regular and irregular waves; for the latter, a general case study in the Black Sea is considered at a Beaufort scale of 6.

4.1.1. Regular waves results

Figure 6 depicts the response amplitude operators for all six Degrees of Freedom (DOF) of the considered vessel in regular waves, at zero speed.

The maximum values for translation motions are recorded for the lower frequency domain. After the value of 1 rad/sec corresponding to an L_{pp}/λ=1.44 i. e. the wave length is approximatively equal to ship length the values for RAO heave become very small. Heave motion has a peak value at 0.8 rad/s, similar to pitch motion.

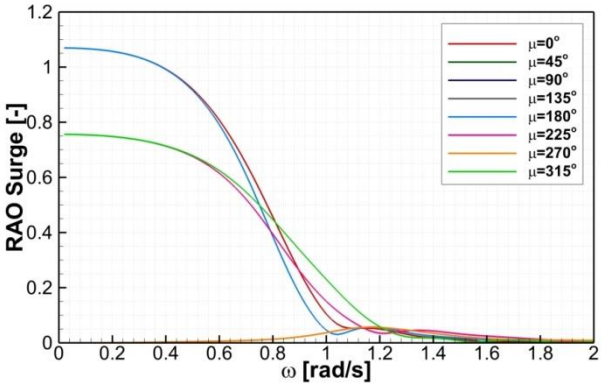

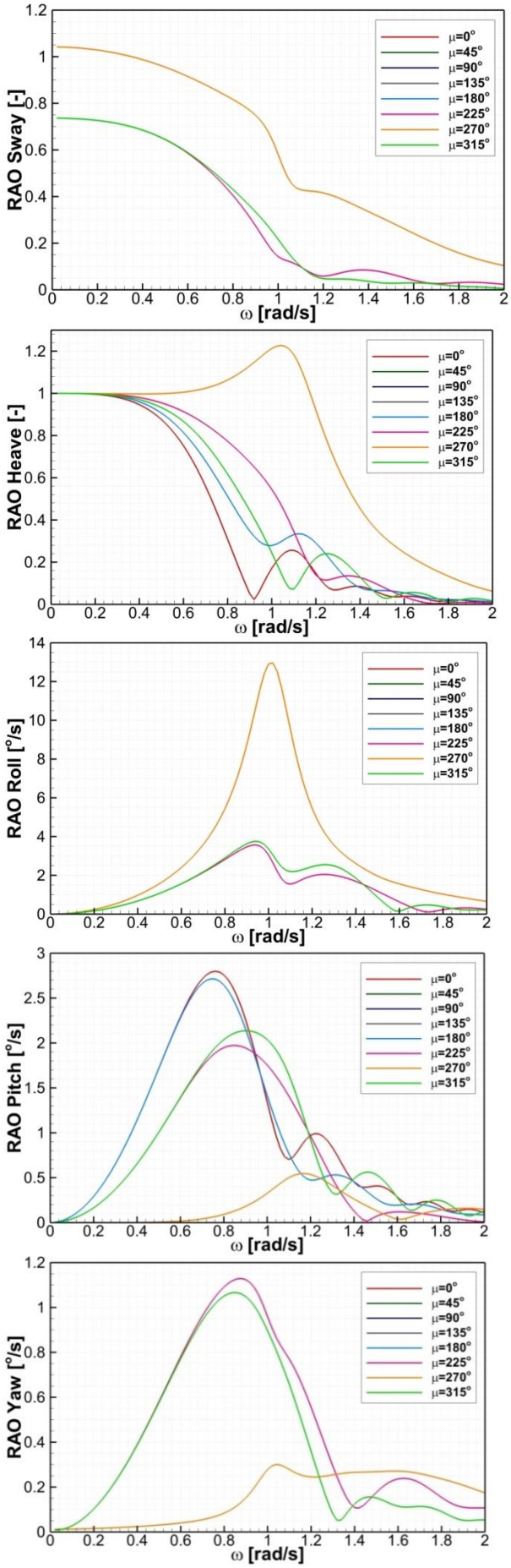

Fig. 6. Ship RAO computed based on BEM method for the 6 DOF at V=0

Since this motion are couple, the vertical bending of ship, if wave induced loads are considered, will have the peak value at the same value of wave circular frequency. Also, it can be observed that for μ=0°and 180° the roll motion has no significant values.

4.1.2. Irregular waves results

The ITTC spectrum is used to represent a general sea condition in the Black Sea at a Beaufort scale of 6, where the corresponding significant wave height is H_S=4m and wind speed V_W is up to 27 knots. This case is considered as the worst case scenario for the operational conditions.

Similarly, the response spectrum for all the 6 DOF is depicted in Figure 7. The results shows that the peak responses are located between the wave frequency ω=0.5~0.8.

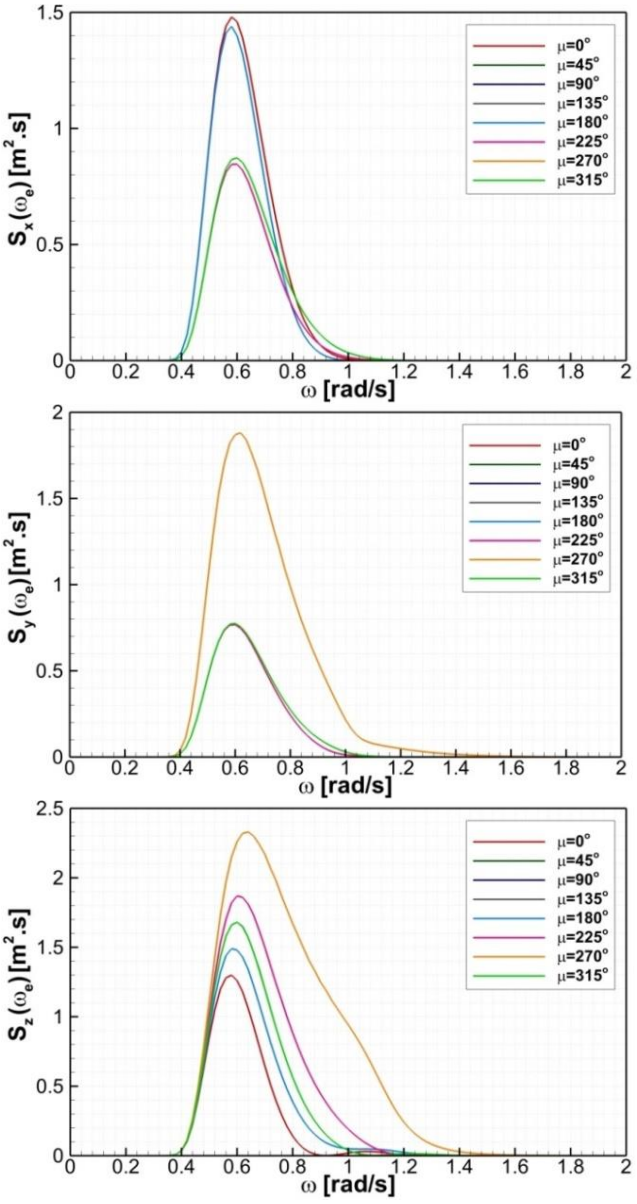

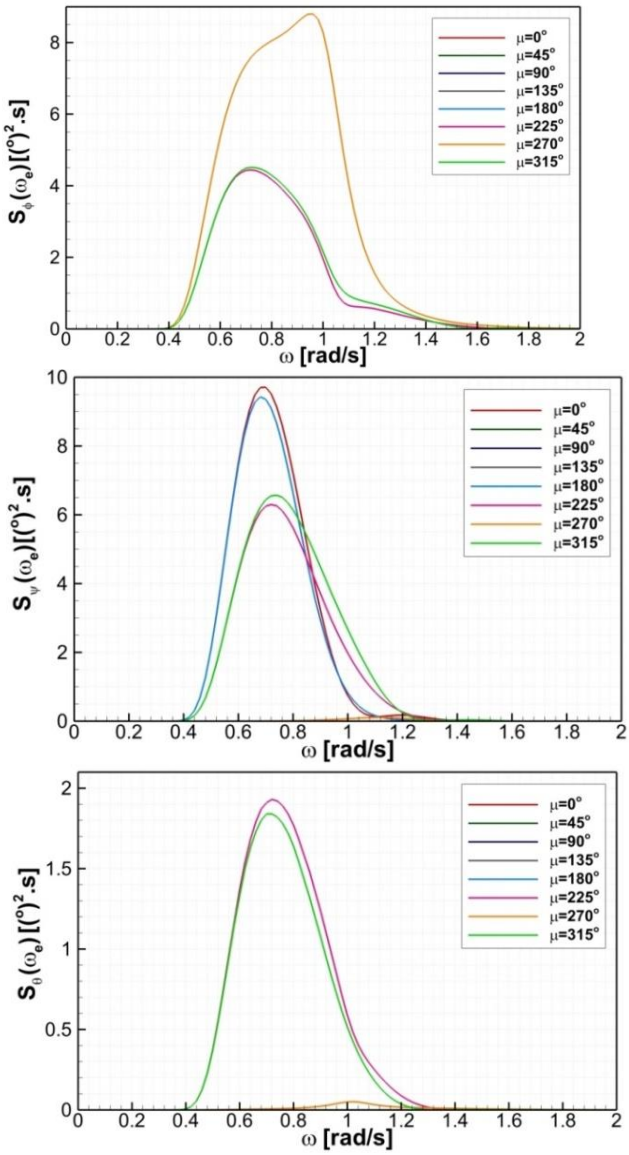

Fig. 7. Response spectrum computed based on BEM method for the 6 DOF at V=0

Head and following seas imposed the maximum surge and pitch responses, beam seas induced the maximum sway, heave and roll reponses and finally the oblique seasshowed to have the most significant yaw response.

The obtained results show that the pitch response is significant and may pose possible green water at the stern. This should be taken into consideration during operational conditions in such a considerably severe sea state for operation by means of mooring lines that limit the pitch motion from the bow and stern.

4.2 URANSE results

One main advantage from the CFD simulations is the possibility of predicting the viscous damping effect for the oscillatory motions and especially for the roll damping effect. For this reason, a comparative case was analyzed for ship sailing at zero speed and 180˚ heading angle where all the 6 DOF are free with the entire hull introduced in the simulation without symmetry assumptions. Simulation is performed until the ship encounters 15 waves according to the ITTC requirements [11]. The time history for the simulation is plotted in Figure 8 shows the response of the ship during wave encounter. The surge motion recorded motion amplitude within 0.4 m and a maximum displacement after 15 wave encounter of 6 m astern. Heave and pitch amplitudes are about 0.5m and 3˚, respectively. The sway and yaw amplitudes are insignificant; it seems to have influence that is apparently coming from the coupled motions. As for the roll motion, which is the main concern, it seems that the amplitude is small the ship continues to incline as the simulation time extends. The behavior is apparently resulting from a parametric rolling effect. This is worthy to be further investigated, and more likely for following sea. This may take place in future studies.

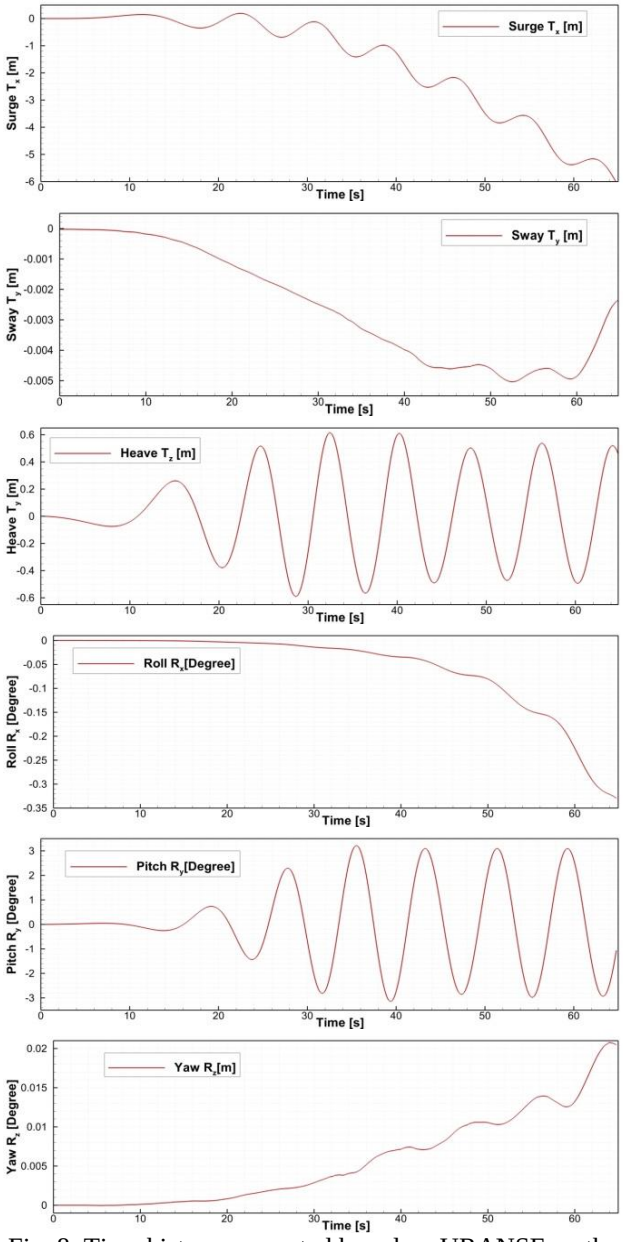

Fig. 8. Time history computed based on URANSE method for the 6 DOF at V=0

It is very important during the seakeeping simulations to study the green water on the deck, especially from the bow and stern, where it is possible for the water to access the deck from both ends during heave, and most likely, pitch motions. To investigate this action, the free-surface configuration and the mass fraction is brought to attention in Figure 9 at the four quarters of the wave, starting from the condition when the peak is at the forward perpendicular F.P. (as the location of the reference encounter point) of the ship, then between peak and trough, when the trough is at the F.P. and finally, between the trough and the peak as schematically illustrated in Figure 9.

It can be observed that in the case when the ship leaves the peak and heads towards the trough, the dissipated peak downstream is interacting with the stern of the ship during the pitching motion and accessing the stern. This can be observed as remained water in the third stage when the ship is at the trough of the wave (as highlighted in red in Figure 6). This recalls the same discussion in the previous section that the pitch motion should be limited in a certain way to avoid the water flooding on the deck during operational conditions.

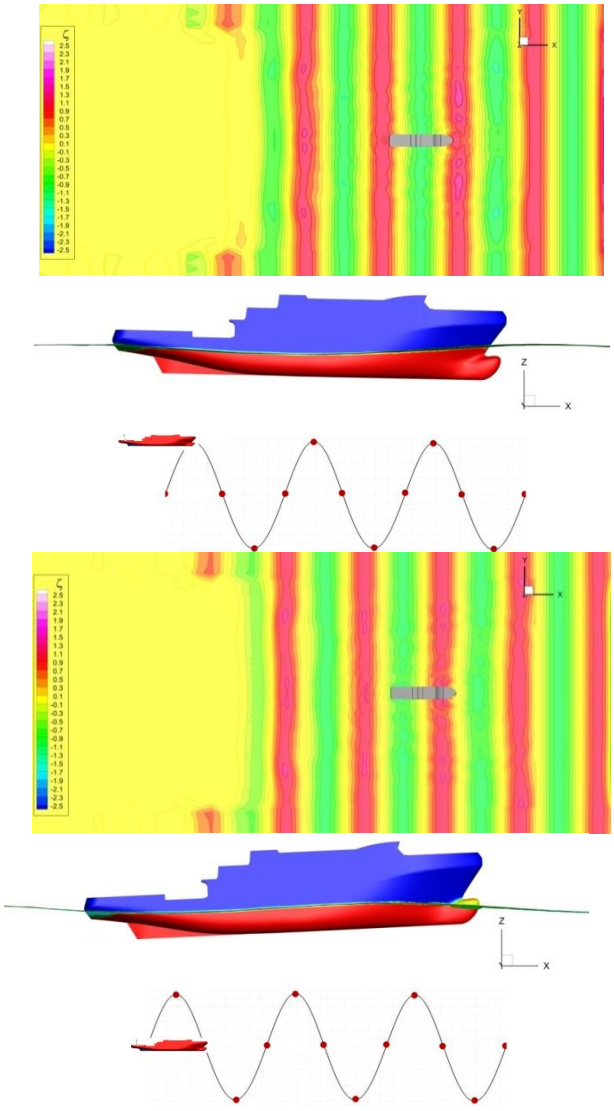

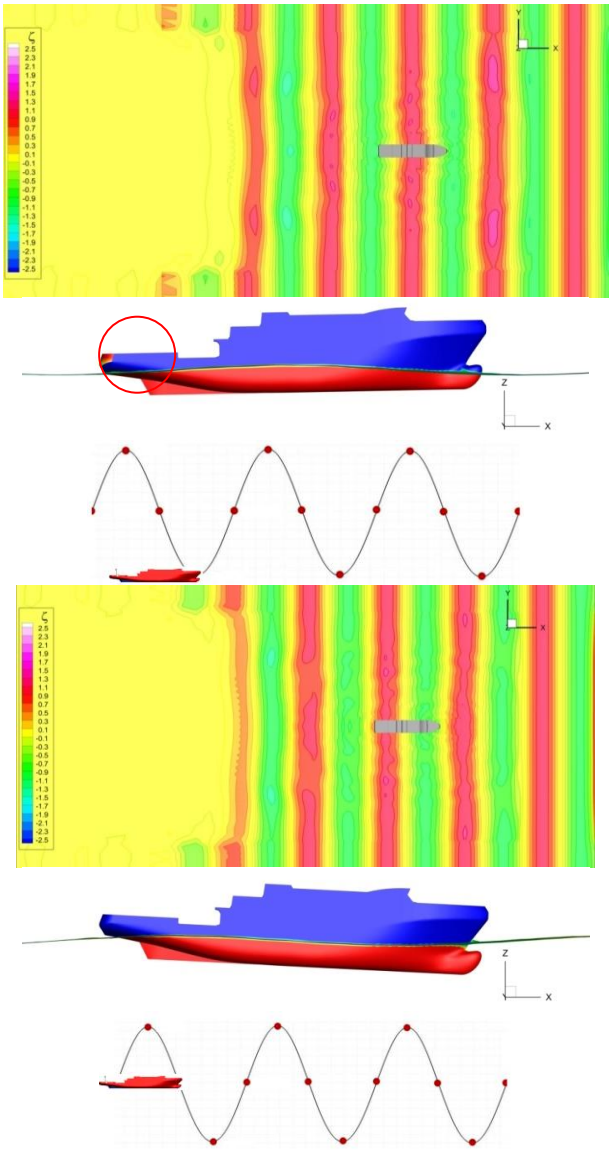

Fig. 9. Wave profile and mass fraction for the four wave quarters

4.3 Results Comparison

The comparison of the both simulation methods is brought to attention in Figure 10, where the surge heave and pitch motions are presented for BEM and URANSE solutions. The results show a well consistency between the methods for surge and heave motions. Nevertheless, for Pitch motion the difference is significant. This might be related to numerical instabilities. Some other explanation might be correlated to the geometry used in both simulations, where in URANSE the full ship is introduced to the computational domain, while in BEM only the immersed part is introduced.

Possible difference regarding the hydrodynamic coefficients may occur due to the analysis method imposed by both approaches. This may require further investigation, since only one point cannot lead to a solid conclusion.

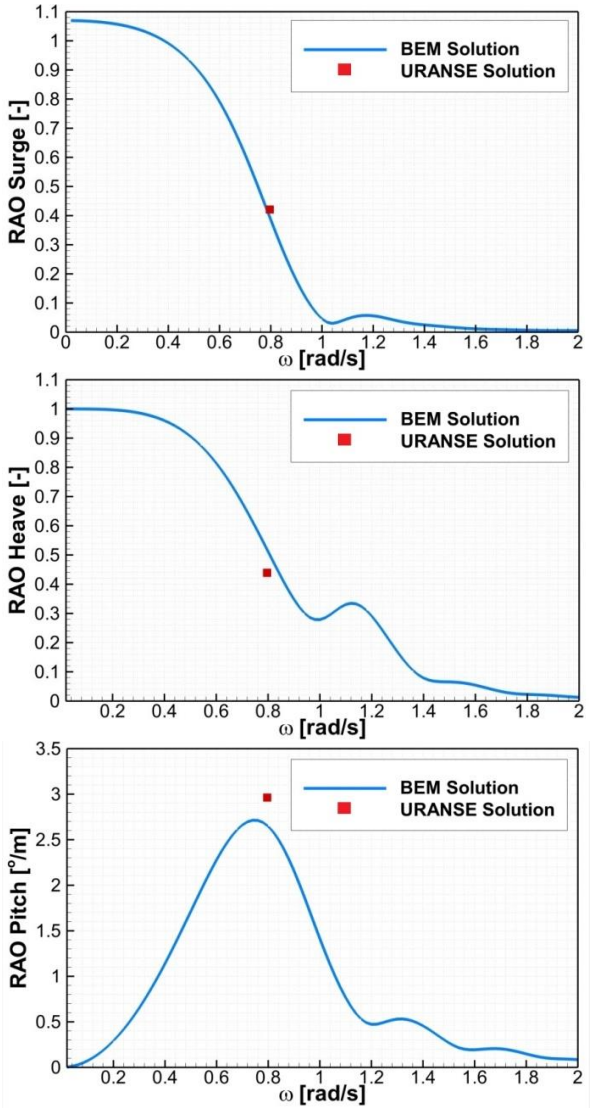

Fig. 10. Comparison between BEM and URANSE results for surge, heave and pitch, respectively

5. CONCLUSIONS

-The hydrodynamic response of an offshore AHTS ship was numerically estimated at the operational condition when the ship speed is equal to zero based on two methods (Boundary Element Method BEM and Unsteady Reynolds-Averaged Navier-Stokes Equations URANSE). For BEM method, the wave frequency range was set to ω=0.2~2.0 rad/s with a step of 0.2, while the ships heading angle was chosen within μ=0~315˚ with a step 15˚. The ship response in regular and irregular waves was predicted and reported for all the 6 DOF at different heading angle. The wave spectrum used for analyzing the ship sailing in real sea was the ITTC spectrum with a general case in the Black Sea corresponding to a Beaufort scale of 6, wind speed is up to 27 knots and the significant wave height is 4m. For the URANSE simulation, only one case was chosen for comparison purposes where the responses obtained in the BEM solution were maximum. In this case, wave length was set to ship length, wave frequency ω=0.2 rad/s and wave amplitude of unity. Having both simulation results we may highlight the following points:

-the BEM simulations showed that the ship has significant responses when the frequency is within the range of ω=0.5~0.8 rad/s, with the peak mainly located at ω=0.8 rad/s.

-maximum surge and pitch responses were recorded for head and folowing seas, while the beam seas imposed the maximum responses for surge, heave and roll, both cases comply with the thoeritical approaches.

-maximum roll angle is within 13˚ recorded for beam seas, while the maximum pitch angle was within 2.53˚ in head waves.

-the spectral response was estimated for the ship in a generic condition, which referes to the extreme operational condition. The pitch response for this case was significant and possible green water could be expected to form on the stern zone. For this reason, it is recommended to insure limiting the pitch motion during operation in such significant sea state by means of mooring lines, for example.

-the URANSE simulation showed a proper prediction for the ship responses for all the 6 DOF with a proper visualization of the flow around the hull, especially for the pitch motion, where the water was visualized greening the stern area during simulation.

-results comparison between BEM and URANSE showed a close coherence between the computed values based on both approaches, especially for surge and heave; nevertheless, the difference for pitch motion was noticeably high. This might be realated to numerical instabilities. Worth mentioning that the simulation performed in BEM has different assumptions than that in URANSE; for example, the whole geometry is presented in the URANSE, while only the immersed part is presented in BEM.

-the simulation cost and time for URANSE is very significant compared to the BEM simulation. Applying the URANSE simulation for multiple cases is still not feasible.

-In general, combining both methods can provide the best practice, especially when the viscous effect is important to be taken into considerations. This work sets the base for further investigations to be carried in the near future by the authors.

6. ACKNOWLEDGEMENTS

The present study was conducted under the framework activities of the Naval Architecture Research Center (CCAN). Also, the author would like to acknowledge the Bureau Veritas.

7. REFERENCES

1. Tezdogan, T., Demirel, Y.K., Kellett, P., Khorasanchi, M., Incecik, A., (2015). *Full-scale unsteady RANS CFD simulations of ship behaviour*

and performance in head seas due to slow steaming, J. Ocean Eng., 97, 186–206.
2. Kim, M., Hizir, O., Turan, O., Incecik, A., (2017). *Estimation of added resistance and ship speed loss in a seaway*, J. Ocean Eng., 140, 466–476.
3. Pacuraru, F., Pacuraru, S., Bekhit, A., (2020). *Numerical analysis of ship motions for an offshore vessel*, AIP Conf. Proc. 2293, 420091, 1–4.
4. Pacuraru F., Domnisoru, L., Pacuraru, S., (2020). *On the comparative seakeeping analysis of the full scale kcs by several hydrodynamic approaches*, J. Mar. Sci. Eng., 8(12), 962, 1–32.
5. Bekhit, A., (2018). *Unsteady RANSE simulation for ship resistance, heave and pitch in regular head waves*, IOP Conf. Ser.: Mater. Sci. Eng., 400(8), 082004.
6. Bekhit, A., Lungu, A., (2019). *Numerical Prediction of the Ship Resistance and Vertical Motions in Regular Head Waves*, Proc. ASME, pp, 1-10, Offshore and Arctic Eng. – OMAE 2019, Scotland (Glasgow).
7. Bureau Veritas, (2020). Hydrostar user manual, 1-192.
8. Guevel, P., Bougis, J., (1982), *Ship-motions with forward speed in infinite depth*, Int. Shipbuilding Progress, 29(332), 103-117.
9. Deng, G.B., Queutey, M., Visonneau, M., (2010). *RANS prediction of the KVLCC2 tanker in head waves*, J. Hydrodynamics, 22(5), 476–481.
10. Queutey, P., Deng, G.B., Wackers, J., Guilmineau, E., Leroyer, A., Visonneau, M., (2012). *Sliding grids and adaptive grid refinement for RANS simulation of ship-propeller interaction*, J. Ship Technology Research, 59(2), 44-58.
11. The seakeeping committee: Final report and recommendations to the 25th ITTC, Proc. 25th ITTC, Vol. I, pp 209- 262.

Received: April 15, 2022 / Accepted: December 15, 2022 / Paper available online: December 20, 2022 © International Journal of Modern Manufacturing Technologies